Summer July 1, 2017

Fine-Grained Reliability for V2V Communications around Suburban and Urban Intersections

Dr. Mouhamed Abdulla, *Chalmers University of Technology, Göteborg, Sweden*
Prof. Henk Wymeersch, *Chalmers University of Technology, Göteborg, Sweden*

Fine-Grained Reliability for V2V Communications around Suburban and Urban Intersections

Mouhamed Abdulla, *Member, IEEE,* and Henk Wymeersch, *Member, IEEE*

Abstract

Safe transportation is a key use-case of the 5G/LTE Rel.15+ communications, where an end-to-end reliability of 0.99999 is expected for a vehicle-to-vehicle V2V transmission distance of 100–200 m. Since communications reliability is related to road-safety, it is crucial to verify the fulfillment of the performance, especially for accident-prone areas such as intersections. We derive closed-form expressions for the V2V transmission reliability near suburban corners and urban intersections over finite interference regions. The analysis is based on plausible street configurations, traffic scenarios, and empirically-supported channel propagation. We show the means by which the performance metric can serve as a preliminary design tool to meet a target reliability. We then apply meta distribution concepts to provide a careful dissection of V2V communications reliability. Contrary to existing work on infinite roads, when we consider finite road segments for practical deployment, fine-grained reliability per realization exhibits bimodal behavior. Either performance for a certain vehicular traffic scenario is very reliable or extremely unreliable, but nowhere in relatively proximity to the average performance. In other words, standard SINR-based average performance metrics are analytically accurate but can be insufficient from a practical viewpoint. Investigating other safety-critical point process networks at the meta distribution-level may reveal similar discrepancies.

The authors are with the Division of Communication and Antenna Systems, Dept. of Electrical Engineering, Chalmers University of Technology, Göteborg, Sweden, e-mails: {mouhamed,henkw}@chalmers.se.

This research work is supported, in part, by the European Commission under the Marie Skłodowska-Curie Individual Fellowship (H2020-MSCA-IF-2014), EU-MARSS-5G project, Grant No. 659933; Ericsson Research Foundation, Grant No. FOSTIFT-16:043-17:054; the VINNOVA COPPLAR project, funded under Strategic Vehicle Research and Innovation Grant No. 2015-04849; and the EU-H2020 HIGHTS project (High Precision Positioning for Cooperative ITS Applications), Grant No. MG-3.5a-2014-636537.

This draft is also available on arXiv, URL: https://arxiv.org/abs/1706.10011.

I. INTRODUCTION

The United Nations World Health Organization estimates that 1.25 million people are fatally injured every year due to road-traffic accidents [1]. Studies conducted by the US Department of Transportation suggests that 2% of crashes are due to vehicle components failure or degradation; another 2% are attributed to the environment and weather conditions, while a staggering 94% is tied to human choice or error, such as careless driving, speeding, and driving under the influence [2]. This alarming reality suggests that human cognition is insufficient in its capacity to maneuver in an intricate transportation system with high reliability. Reliance on augmented technology is thus needed to compensate for the limitations of human drivers. Eventually, highly automated vehicles (HAV) will operate in self-driving capability through 360-degree awareness of their surroundings via artificial intelligence, machine learning and cooperative communications.

Present manifestations of autonomous vehicles rely predominantly on radars, cameras, LiDARs, ultrasonic sensors, GPS, and cloud-based vehicle-to-network 3D digital mapping. Sensor-based autonomous vehicles are, however, constrained by line-of-sight, and their effectiveness is significantly influenced by weather conditions, such as fog, sunbeams, heavy rain and snow. Meanwhile, vehicle-to-vehicle (V2V) communications is the *only* HAV-related technology that has the capacity to *see around corners* in the presence of urban structures. Moreover, V2V communications is more reliable than sensors in harsh weather conditions. Although current efforts are still at the research phase, dynamically formed vehicular ad hoc network (VANET) will inevitably be included within the HAV ecosystem. Evidently, the addition of V2V capability as a complementary technology and as a supplemental source of system redundancy is expected to improve the reliability of machine-driven units and, as a consequence, further shrink the likelihood of accidents by HAV-systems [3], [4]. And this is not surprising, given that standalone V2V technology is estimated to prevent up to 35% of serious road accidents [5].

There are various V2V use-cases that require careful investigation and analysis for the purpose of enhancing road-safety and traffic efficiency. Data assessed between 2010 to 2015 suggest that the nearly half of all vehicular accidents occur at intersections [6]. Despite vehicular high-densification and greater proliferation of accident avoidance technology, it is surprising to note that the rate of intersection accidents remained consistent year after year. These numbers reveal that intersection-related accidents are high consequence events that occur with a very high probability. Thus, carefully studying the reliability of V2V communications around intersections,

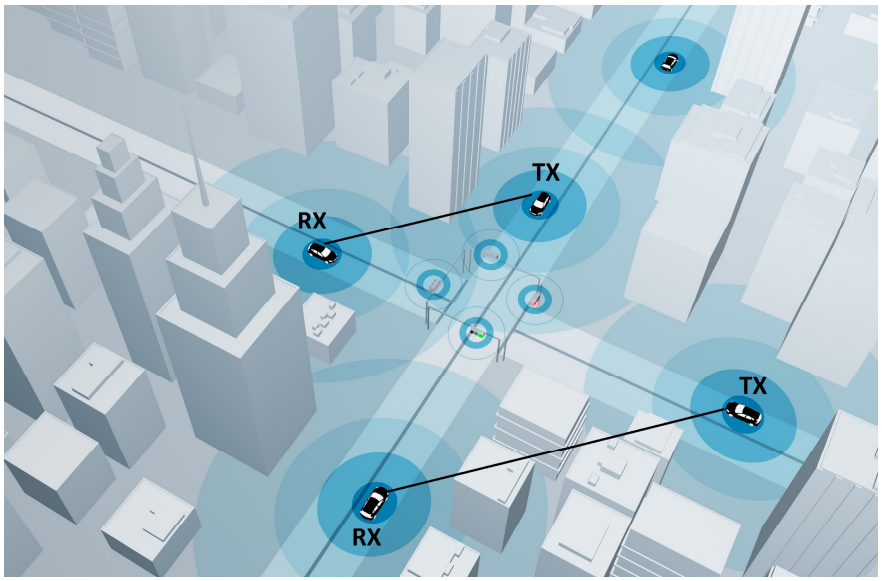

Fig. 1. Intelligent V2V wireless communications of safety-critical data by a pair of vehicles maneuvering around a built-up blind urban intersection, whereby a transmitter (TX) sends data packets to a receiver (RX), in the presence of simultaneous interferers (source: image adapted from and used with permission from Volvo Car Group, Public Affairs, SE-405 31, Göteborg, Sweden).

and in particular blind urban junctions where the loss due RF propagation is of major concern (see Fig. 1), will help us assess the feasibility of seeing non-line-of-sight vehicles near corners.

A. Enabling Technology

To ensure effective scalability and interoperability among radio units mounted on vehicles, standardization is of utmost importance. Today, there are two competing standards: (i) IEEE 802.11p, commonly known as direct short range communication (DSRC)[1] [7]; and (ii) cellular-V2X (C-V2X)[2] connectivity supported by 4G/LTE Rel.14+ [8]–[10]. The competition among these two standards is still fluid and continuously evolving. Granted, the locally-based DSRC standard is defined and ready for utilization, whereas the network-based C-V2X is still under development for 5G/LTE Rel.15+ operation aimed around 2020. Meanwhile, HAV-systems will rely on machine learning capability, where hours of driving experience will serve as an acquisition

[1]DSRC for dynamic vehicles relatively resembles the popular Wi-Fi (IEEE 802.11) standard utilized for quasi-stationary wireless connectivity.

[2]C-V2X also supports direct VANET communication (i.e., similar to DSRC) without necessarily relying on network involvement for scheduling.

mechanism of observing and learning from experience. Newly acquired knowledge will then be shared wirelessly to the cloud and to other units using V2X capability at high data rates. Other vehicles will immediately upgrade their knowledge-based system regarding the transportation status and aggregate experience of certain geographical regions without the need for further acquisition time.

Communicating real-time big data generated by HAVs will require the potential of 5G broadband connectivity where a peak data rate of 10 Gbps is projected [11]. It is reassuring to know that such multi-Gbps transmission is envisioned and possible using technologies such as mmWave communications [12], [13]. Moreover, C-V2X is expected to deliver a larger communications range; by some estimates twice the distance of DSRC for a fixed reliability value. Further, the reliability under 5G performs significantly better than DSRC [14]. Also, greater mobility of up to 500 km/hr is supported. Overall, the reliance on C-V2X operating with 5G seems promising and quite compatible with the requirements of HAV-systems.

B. Problem Statement and Contribution

Ultimately, we need to develop analytical expressions that will serve as a mechanism to quantify the extent of reliability for a certain V2V communication link and eventually aid in identifying the contribution of relevant parameters for the purpose of network design. Analytical modeling based on point processes is well suited to study such problems where techniques from stochastic geometry have been applied to vehicular communications (e.g. [15]–[23]). As for intersections, they were explicitly considered in [18], though only for suburban/rural scenarios over infinitely long roads. For the analytical expressions to have practical real-world relevance, they must build on plausible VANET scenarios coupled with channel models validated by extensive measurement campaigns [24], [25]. The above-mentioned works in stochastic geometry allow the evaluation of the *average reliability*, obtained by averaging over different fading realizations and node placements. This average reliability may obscure the performance for specific node configuration [26], referred to as the *fine-grained reliability*.

In this paper, we perform a study of average and fine-grained reliability, dedicated to urban intersections, which have particular propagation characteristics [27]–[30], complementing and generalizing the results in [18] and [23]. The key contributions of this paper are summarized as follows:

1) We evaluate the transmission reliability as a function of system parameters, vehicular traffic, infrastructure geometry, and empirically-validated V2V channel propagation models geared for suburban and urban intersections. The analysis is generic and allows for closed-form expressions over finite road segments of practical significance for real-world deployment.
2) While considering a large number of design parameters embedded within the derived reliability metrics, we demonstrate the approach for re-configuring the VANET in order to ascertain a target reliability.
3) Using extensive Monte Carlo simulation techniques, we show the fine-grained V2V reliability obtained through the meta distribution. Although analytically accurate, the discrepancy between average reliability and fine-grained reliability is substantial from a practical standpoint. The most striking observation is that average reliability provides an oversimplified distortion of the actual communication performance incurred by each vehicular traffic realization under the specified VANET scenario.

C. Organization

The rest of the paper is organized as follows. In Section II, we outline the considered VANET network traffic and geometry and describe the specialized intersection-based channel models for V2V communications under line-of-sight (LOS), weak-line-of-sight (WLOS), and non-line-of-sight (NLOS) scenarios. Then, in Section III, we dissect the stipulated requirements for reliability in 5G communications; we provide an analytical definition for reliability and relate it to its average; we also explain the notion of fine-grained reliability. Closed-form performance measures for different channel environments are subsequently derived in Section IV and applied to network design in order to meet a preset target performance. Furthermore, in Section V, we display results from fine-grained reliability based on extensive Monte Carlo simulations of the meta distribution, and we discuss its unexpected relation to standard reliability assessment obtained through averages. Finally, we conclude the paper with Section VI.

II. System Model

A. Network Model

The analysis is based on VANET formed near suburban corners and blind urban intersections, where the network traffic and geometry is described as follows. The transmitter (TX) can be located anywhere on the horizontal or vertical road, and the receiver (RX), which, without loss

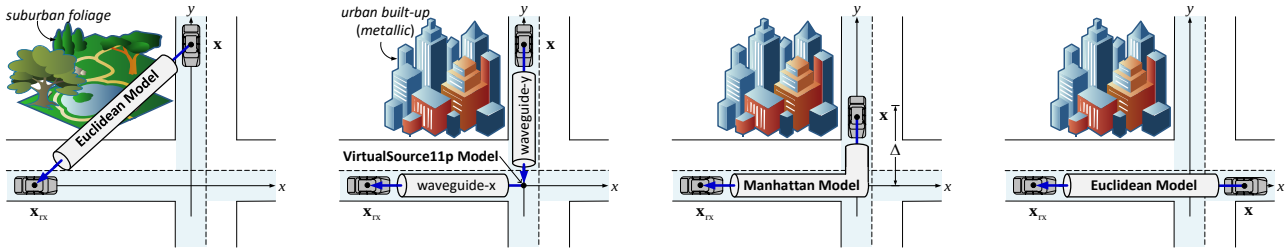

(a) suburban channel: LOS/WLOS (b) urban channel: NLOS (c) urban channel: WLOS (d) urban channel: LOS

Fig. 2. Propagation models for different V2V channel environments as a function of vehicular positions around suburban corners and blind urban intersections.

of generality, is confined to the horizontal road. Hence, $\mathbf{x}_{\rm tx} = x_{\rm tx}\mathbf{e}_{\rm x} + y_{\rm tx}\mathbf{e}_{\rm y}$ and $\mathbf{x}_{\rm rx} = x_{\rm rx}\mathbf{e}_{\rm x}$, where $x_{\rm tx}, x_{\rm rx}, y_{\rm tx} \in \mathbb{R}$, such that $x_{\rm tx}y_{\rm tx} = 0$, where $\mathbf{e}_{\rm x} = [1\,0]^{\rm T}$, $\mathbf{e}_{\rm y} = [0\,1]^{\rm T}$. Other vehicles are randomly positioned on both horizontal and vertical roads and follow a homogeneous Poisson point process (H-PPP) over bounded sets $\mathcal{B}_{\rm x} = \left\{x \in \mathbb{R} \middle| |x| \leq R_{\rm x}\right\}$ and $\mathcal{B}_{\rm y} = \left\{y \in \mathbb{R} \middle| |y| \leq R_{\rm y}\right\}$, such that $R_{\rm x} > 0$ and $R_{\rm y} > 0$ are road segments of the intersection region, and the vehicular traffic intensities are respectively given by $\lambda_{\rm x}$ and $\lambda_{\rm y}$. Moreover, interfering vehicles follow an Aloha MAC protocol[3] and can transmit independently with a probability $p_{\rm I} \in [0, 1]$. In the rest of the paper, the following shorthand notations are accordingly used to refer to the geometry of interfering vehicles on each road, modeled by thinned H-PPPs

$$\Phi_{\rm x} = \{\mathbf{x}_i\}_{i=1,2,\ldots,n} \in \mathbb{R}^n \sim \text{PPP}\left(p_{\rm I}\lambda_{\rm x}, \mathcal{B}_{\rm x}\right) \tag{1}$$

$$\Phi_{\rm y} = \{\mathbf{x}_j\}_{j=1,2,\ldots,m} \in \mathbb{R}^m \sim \text{PPP}\left(p_{\rm I}\lambda_{\rm y}, \mathcal{B}_{\rm y}\right), \tag{2}$$

such that n and m are random Poisson distributed integers with mean $p_{\rm I}\lambda\,|\mathcal{B}|$, where $|\mathcal{B}|$ is the Lebesgue measure of bounded set $\mathcal{B}$. All vehicles, including TX, broadcast with the same power level $P_{\circ}$. The receiver signal-to-interference-plus-noise-ratio (SINR) threshold for reliable detection is set to β, in the presence of additive white Gaussian noise (AWGN) with power $N_{\circ}$. The SINR depends on the propagation channel, described next.

[3]Resource selection for DSRC is based on CSMA with collision avoidance; and C-V2X defined by 3GPP-PC5 interface relies on semi-persistent transmission with relative energy-based selection. Nonetheless, for the purpose of preliminary analysis, we here only consider the Aloha MAC protocol.

B. Channel Models

The detected power observed at the RX from an active transmitting vehicle at location $\mathbf{x}$ is modeled by $P_{\mathrm{rx}}(\mathbf{x}, \mathbf{x}_{\mathrm{rx}}) = P_{\circ}\ell_{\mathrm{ch}}(\mathbf{x}, \mathbf{x}_{\mathrm{rx}})$, which depends on transmit power $P_{\circ}$ and channel losses $\ell_{\mathrm{ch}}(\mathbf{x}, \mathbf{x}_{\mathrm{rx}})$. The channel losses consist of three components: average path loss $\ell_{\mathrm{pl}}(\mathbf{x}, \mathbf{x}_{\mathrm{rx}})$ that captures the propagation losses, shadow fading $\ell_{\mathrm{s}}(\mathbf{x}, \mathbf{x}_{\mathrm{rx}})$ that captures the effects of random channel obstacles, and random small-scale fading $\ell_{\mathrm{f}}(\mathbf{x})$ that captures the non-coherent addition of signal components. For the purpose of tractability, we implicitly consider shadow fading to be inherent within the H-PPP, and thus regard $\ell_{\mathrm{ch}}(\mathbf{x}, \mathbf{x}_{\mathrm{rx}}) \simeq \ell_{\mathrm{pl}}(\mathbf{x}, \mathbf{x}_{\mathrm{rx}})\,\ell_{\mathrm{f}}(\mathbf{x})$ [31], [32]. We model $\ell_{\mathrm{f}}(\mathbf{x}) \sim \mathrm{Exp}(1)$ as Rayleigh fading, independent with respect to $\mathbf{x}$. The path loss $\ell_{\mathrm{pl}}(\mathbf{x}, \mathbf{x}_{\mathrm{rx}})$ for different channel environments is described below.

1) Suburban/Rural Channel: As shown on Fig. 2a, the average path loss model that is generally considered for V2V propagation adheres to an inverse power-law [24], [25]; thus

$$\ell^{\mathrm{s}}_{\mathrm{pl}}(\mathbf{x}, \mathbf{x}_{\mathrm{rx}}) = A_{\circ}\left\|\mathbf{x}_{\mathrm{rx}} - \mathbf{x}\right\|^{-\alpha} \quad \mathbf{x} \neq \mathbf{x}_{\mathrm{rx}}. \tag{3}$$

In this expression, $\|\cdot\|$ is the l_2-norm, $A_{\circ}$ corresponds to the LOS/WLOS path loss coefficient, which is primarily a function of operating frequency $f_{\circ}$, path loss exponent $\alpha > 1$, reference distance $d_{\circ}$, and antenna heights $h(\mathbf{x})$ and $h(\mathbf{x}_{\mathrm{rx}})$.

2) Urban Channel: For metropolitan intersections where the concentration of high-rise and impenetrable metallic-based buildings and structures are prevalent, the previous model is rather unrealistic. As a consequence, a specialized channel predictor is required. Real-world measurements of V2V communications operating at 5.9 GHz were conducted at different urban intersection locations within the city of Munich, Germany. This led to the development of the VirtualSource11p path loss model [29], where the name refers to a virtual-relay at the junction point. A subsequent study conducted in Lund, Sweden independently validated the accuracy of this model [30]. As a result, it serves as inspiration to our simplified model that accounts for all possible channel occurrences as vehicles navigate around the intersection

$$\ell^{\mathrm{u}}_{\mathrm{pl}}(\mathbf{x}, \mathbf{x}_{\mathrm{rx}}) = \tag{4}$$
$$\begin{cases} A'_{\circ}\left(\|\mathbf{x}\| \cdot \|\mathbf{x}_{\mathrm{rx}}\|\right)^{-\alpha} & \min\left(\|\mathbf{x}\| = |y|, \|\mathbf{x}_{\mathrm{rx}}\|\right) > \triangle \\ A_{\circ}\left(\|\mathbf{x}\| + \|\mathbf{x}_{\mathrm{rx}}\|\right)^{-\alpha} & \min\left(\|\mathbf{x}\| = |y|, \|\mathbf{x}_{\mathrm{rx}}\|\right) \leq \triangle \\ A_{\circ}\left\|\mathbf{x}_{\mathrm{rx}} - \mathbf{x}\right\|^{-\alpha} & \|\mathbf{x}\| = |x|;\ \mathbf{x} \neq \mathbf{x}_{\mathrm{rx}}. \end{cases}$$

As depicted in Fig. 2b, the first case refers to the VirtualSource11p model, where $\mathbf{x} = y\mathbf{e}_{\mathrm{y}}$ is in NLOS, orthogonal to the RX. The second case refers to the Manhattan model for WLOS when either TX/interferer or RX are close to the intersection; this is characterized by the break-point distance $\triangle$ as shown in Fig. 2c, typically on the order of the road width. The third case refers to the standard Euclidean model, where $\mathbf{x} = x\mathbf{e}_{\mathrm{x}}$ is in LOS, on the same road as the RX as shown in Fig. 2d. Meanwhile, since the propagation under NLOS is more severe than the cases under LOS/WLOS, then the NLOS path loss coefficient $A'_{\circ}$ should generally satisfy the condition that $A'_{\circ} < A_{\circ}\left(\triangle/2\right)^{\alpha}$, where the determination of $A_{\circ}$ was described earlier.

Remark 1. The model in (4) exhibits discontinuities. A mixture (a linear weighting) of these models can be used to avoid these discontinuities, though this is not considered in this paper.

Remark 2. We will only consider the plausible case where the region of H-PPP interferers is greater or equal than the path loss break-point distance, i.e., $\min\left(R_{\mathrm{x}}, R_{\mathrm{y}}\right) \geq \triangle$.

III. Generalized Transmission Reliability

For road-safety purposes, a 5G reliability of 10^{-5} is required up to transmission distance of $200\,\mathrm{m}$ in the suburbs, and $100\,\mathrm{m}$ in urban settings [33]. With limited cross-layer optimization, this end-to-end requirement can be dissected as follows: $10^{-2} \sim 10^{-3}$ at the physical (PHY) layer; 10^{-4} at the MAC layer (with at most $2 \sim 3$ low-latency retransmissions); and 10^{-5} at the network layer. Such reliability categorization is generally consistent for semi-autonomous vehicles operating with dual LiDAR/V2X capabilities. Full autonomy will require stringent ultra-high reliability in the range of $10^{-7} \sim 10^{-9}$. To assess these values for different VANET scenarios, we require: (i) a definition for reliability, and (ii) a general evaluation mechanism for reliability.

A. Defining Reliability

There are multiple ways to define reliability, the most prevalent among them are:

- *Rate Coverage Probability*: This metric, suitable for long packets, refers to the likelihood that the achievable rate $R_{\mathrm{ar}} = B\log_2\left(1+\mathsf{SINR}\right)$ (measured in bits per seconds) at the RX, where B is the bandwidth of the communication link, is larger than a threshold r_{th}; i.e., $\Pr\left(R_{\mathrm{ar}} \geq r_{\mathrm{th}}\right) = \Pr\left(\mathsf{SINR} \geq \beta\right)$, such that the SINR threshold corresponds to $\beta \triangleq 2^{r_{\mathrm{th}}/B} - 1$. The link layer outage probability is defined as: $1 - \Pr\left(\mathsf{SINR} \geq \beta\right)$.

- *Maximum Coding Rate*: This metric, suitable for short packets, is a function of the finite packet length $n_{\mathrm{p}} \simeq BT$, where T is the transmission duration; and finite packet error rate (PER) ϵ_{p}. The rate is approximated by $R^{*}\left(n_{\mathrm{p}}, \epsilon_{\mathrm{p}}\right) \simeq R_{\mathrm{ar}} - \sqrt{V/n_{\mathrm{p}}} Q^{-1}\left(\epsilon_{\mathrm{p}}\right)$, where $Q^{-1}\left(\cdot\right)$ is the inverse of the Gaussian Q-function and V is channel dispersion [34], [35]. In other words, to sustain a target PER over a finite packet size, a penalty is incurred to the achievable rate.

Although the maximum coding rate is a generalization of the rate coverage probability, analysis in conjunction with point processes is yet to be developed. As a result, we will consider the rate coverage definition for reliability, detailed next.

B. Average Reliability

Our goal is to determine the success probability $\mathcal{P}_{\mathrm{c}}\left(\beta, \mathbf{x}_{\mathrm{tx}}, \mathbf{x}_{\mathrm{rx}}\right) \triangleq \Pr\left(\mathsf{SINR} \geq \beta\right)$, where $\Pr\left(\cdot\right)$ is averaged over small-scale fading of the wanted link $\ell_{\mathrm{f}}\left(\mathbf{x}_{\mathrm{tx}}\right)$ and point processes Φ_{x} and Φ_{y}; and where

$$\mathsf{SINR} = \frac{\ell_{\mathrm{f}}\left(\mathbf{x}_{\mathrm{tx}}\right) \ell_{\mathrm{pl}}\left(\mathbf{x}_{\mathrm{tx}}, \mathbf{x}_{\mathrm{rx}}\right)}{\sum\limits_{\mathbf{x} \in \Phi_{\mathrm{x}} \cup \Phi_{\mathrm{y}}} \ell_{\mathrm{f}}\left(\mathbf{x}\right) \ell_{\mathrm{pl}}\left(\mathbf{x}, \mathbf{x}_{\mathrm{rx}}\right) + \gamma_{\circ}}, \tag{5}$$

in which $\gamma_{\circ} = N_{\circ}/P_{\circ}$. We introduce a normalized aggregate interference associated with some process Φ as: $I\left(\Phi\right) \triangleq \sum_{\mathbf{x} \in \Phi} \ell_{\mathrm{f}}\left(\mathbf{x}\right) \ell_{\mathrm{pl}}\left(\mathbf{x}, \mathbf{x}_{\mathrm{rx}}\right)$. After isolating for the exponentially distributed fading of the useful signal, and taking the expectation of the probability with respect to interference, we obtain

$$\begin{aligned}\mathcal{P}_{\mathrm{c}}\left(\beta, \mathbf{x}_{\mathrm{tx}}, \mathbf{x}_{\mathrm{rx}}\right) = \underbrace{\exp\left(-\beta' \gamma_{\circ}\right)}_{\triangleq\ \mathcal{P}_{\mathrm{noint}}} \times \underbrace{\mathbb{E}_{I_{\mathrm{x}}}\left\{\exp\left(-\beta' I\left(\Phi_{\mathrm{x}}\right)\right)\right\}}_{\triangleq\ \mathcal{P}_{\circ}(\Phi_{\mathrm{x}})} \\ \times \underbrace{\mathbb{E}_{I_{\mathrm{y}}}\left\{\exp\left(-\beta' I\left(\Phi_{\mathrm{y}}\right)\right)\right\}}_{\triangleq\ \mathcal{P}_{\circ}(\Phi_{\mathrm{y}})},\end{aligned} \tag{6}$$

where $\beta' = \beta/\ell_{\mathrm{pl}}\left(\mathbf{x}_{\mathrm{tx}}, \mathbf{x}_{\mathrm{rx}}\right)$, $\mathcal{P}_{\mathrm{noint}}$ is the success probability in the absence of interference, $\mathcal{P}_{\circ}\left(\Phi_{\mathrm{x}}\right)$ and $\mathcal{P}_{\circ}\left(\Phi_{\mathrm{y}}\right)$ are respectively the degradation of the success probability due to independent aggregate interference from the horizontal and vertical roads, where these two factors can be evaluated by [23]

$$\mathcal{P}_{\circ}\left(\Phi_{\mathrm{q}}\right) = \exp\left(-\int_{\mathcal{B}} \frac{p_{\mathrm{I}} \lambda}{1 + 1/\left(\beta' \ell_{\mathrm{pl}}\left(\mathbf{x}, \mathbf{x}_{\mathrm{rx}}\right)\right)} \mathrm{d}\left(\mathbf{x}^{\mathrm{T}} \mathbf{e}_{\mathrm{q}}\right)\right), \ \mathrm{q} \in \{\mathrm{x}, \mathrm{y}\}. \tag{7}$$

C. Fine-grained Reliability

The success probability $\mathcal{P}_{\rm c}\left(\beta, \mathbf{x}_{\rm tx}, \mathbf{x}_{\rm rx}\right)$ provides a high-level performance assessment averaged over all possible vehicular traffic realizations and channel. Unpacking this average reliability and looking at it at the fine-grained or meta-level demands that we study the success probability of the individual links. In other words, we need to explore the *meta distribution* of the SINR [26]; defined, using the Palm probability $\mathbb{P}^o\left(\cdot\right)$, as

$$F_{\rm r}\left(\beta, p\right) \triangleq \mathbb{P}^o\Big(\Pr\left(\mathsf{SINR} \geq \beta \,|\, \Phi_{\rm x} \cup \Phi_{\rm y}\right) \geq p \Big) \tag{8}$$

Introducing $p_{\rm c}\left(\beta\right) \triangleq \Pr\left(\mathsf{SINR} \geq \beta \,|\, \Phi_{\rm x} \cup \Phi_{\rm y}\right)$ and $p_{\rm out}\left(\beta\right) = 1 - p_{\rm c}\left(\beta\right)$ as the conditional success probability and conditional outage probability, respectively, given the point process $\Phi_{\rm x} \cup \Phi_{\rm y}$, and where $p \in [0, 1]$ is a conditional success reliability constraint. Thus, the meta distribution $F_{\rm r}\left(\beta, p\right)$ is the fraction of vehicular traffic realizations that achieve reliability, where reliability is prescribed by the target value assigned to p, and β is the threshold for SINR.

The average reliability of success can be obtained from $F_{\rm r}\left(\beta, p\right)$ as follows: using the Palm expectation $\mathbb{E}^o\left(\cdot\right)$, we can obtain the moments of $p_{\rm c}\left(\beta\right)$, the first being the average reliability of success, i.e., $\mathbb{E}^o\left(p_{\rm c}\left(\beta\right)\right) = \mathcal{P}_{\rm c}\left(\beta, \mathbf{x}_{\rm tx}, \mathbf{x}_{\rm rx}\right)$. Rather than obtaining the exact meta distribution through the Gil-Pelaez theorem [36], the moments could be used to approximate $F_{\rm r}\left(\beta, p\right)$, where the beta distribution (which only requires the first and second moments) is reported to yield high accuracy [26], [37], [38].

IV. Explicit Reliability for Different Channels

In this section, we are interested to tailor the average reliability metrics for communications specified by the related vehicular propagation models for suburban and urban intersections.

A. Reliability for Suburban Intersections

The channel model of (3) can be applied to the success probability in (6). The impact of random interferers on roads-x and y are accordingly provided by the following propositions.

Proposition 1. The function $\mathcal{P}_{\circ}\left(\Phi_{\mathrm{x}}\right)=\exp\left(-p_{\mathrm{I}}\lambda_{\mathrm{x}}\zeta_{\mathrm{s}}\mathcal{X}\left(R_{\mathrm{x}}\right)\right)$, where $\mathcal{X}\left(R_{\mathrm{x}}\right)$ due to bounded PPP interferers on road-x tailored for suburban intersection evaluates to

$$\begin{aligned}\mathcal{X}\left(R_{\mathrm{x}}\right)=&\,g_{\circ}\Big(\alpha,\big(R_{\mathrm{x}}+\|\mathbf{x}_{\mathrm{rx}}\|\big)/\zeta_{\mathrm{s}}\Big)\\&+g_{\circ}\Big(\alpha,\big(R_{\mathrm{x}}-\|\mathbf{x}_{\mathrm{rx}}\|\big)/\zeta_{\mathrm{s}}\Big)\mathbf{1}_{\|\mathbf{x}_{\mathrm{rx}}\|\leq R_{\mathrm{x}}}\\&-g_{\circ}\Big(\alpha,-\big(R_{\mathrm{x}}-\|\mathbf{x}_{\mathrm{rx}}\|\big)/\zeta_{\mathrm{s}}\Big)\mathbf{1}_{\|\mathbf{x}_{\mathrm{rx}}\|>R_{\mathrm{x}}},\end{aligned}\tag{9}$$

where $\zeta_{\mathrm{s}}=\beta^{1/\alpha}\left\|\mathbf{x}_{\mathrm{rx}}-\mathbf{x}_{\mathrm{tx}}\right\|$, the function $g_{\circ}\left(\alpha,\vartheta\right)$ is defined in (A.4), and in which $\mathbf{1}_{\mathsf{Q}}=1$ when the statement Q is true and 0 otherwise.

Proof: See Appendix A. ■

Proposition 2. The function $\mathcal{P}_{\circ}\left(\Phi_{\mathrm{y}}\right)=\exp\left(-p_{\mathrm{I}}\lambda_{\mathrm{y}}\zeta_{\mathrm{s}}\mathcal{Y}\left(R_{\mathrm{y}}\right)\right)$, where $\mathcal{Y}\left(R_{\mathrm{y}}\right)$ due to bounded PPP interferers on road-y tailored for suburban intersection evaluates to

$$\mathcal{Y}\left(R_{\mathrm{y}}\right)=h_{\circ}\left(\alpha,\left(\left\|\mathbf{x}_{\mathrm{rx}}\right\|/\zeta_{\mathrm{s}}\right)^{2},\left(R_{\mathrm{y}}/\zeta_{\mathrm{s}}\right)^{2}\right),\tag{10}$$

where $\zeta_{\mathrm{s}}=\beta^{1/\alpha}\left\|\mathbf{x}_{\mathrm{rx}}-\mathbf{x}_{\mathrm{tx}}\right\|$, and the function $h_{\circ}\left(\alpha,\delta,\vartheta\right)$ is defined in (B.3).

Proof: See Appendix B. ■

Remark 3. Studies have shown that in suburban environments, $\alpha=2$ is appropriate for inter-vehicular Euclidean distances below 100 m, and $\alpha=4$ for distances beyond [24]. As is detailed in Appendix A-B, both $g_{\circ}\left(\alpha,\vartheta\right)$ and $h_{\circ}\left(\alpha,\delta,\vartheta\right)$ have exact closed-form expressions for $\alpha=2$.

Remark 4. Rather than a bounded region, we may evaluate the success probability impacted, in the aggregate, by infinite H-PPP interferers. Say, we denote the degradation along roads-x and y by $\mathcal{P}_{\circ}^{\infty}\left(\Phi_{\mathrm{x}}\right)=\exp\left(-p_{\mathrm{I}}\lambda_{\mathrm{x}}\zeta_{\mathrm{s}}\mathcal{X}_{\infty}\right)$ and $\mathcal{P}_{\circ}^{\infty}\left(\Phi_{\mathrm{y}}\right)=\exp\left(-p_{\mathrm{I}}\lambda_{\mathrm{y}}\zeta_{\mathrm{s}}\mathcal{Y}_{\infty}\right)$, where $\mathcal{X}_{\infty}$ and $\mathcal{Y}_{\infty}$ are determined by taking the limit of (9) and (10) as R_{x} and R_{y} tend to infinity

$$\mathcal{X}_{\infty}=2\pi\csc\big(\pi/\alpha\big)/\alpha\tag{11}$$

$$\mathcal{Y}_{\infty}=\begin{cases}\lim_{\vartheta\to\infty}h_{\circ}\left(\alpha,\left(\left\|\mathbf{x}_{\mathrm{rx}}\right\|/\zeta_{\mathrm{s}}\right)^{2},\vartheta\right) & \left\|\mathbf{x}_{\mathrm{rx}}\right\|\neq 0\\ 2\pi\csc\big(\pi/\alpha\big)/\alpha & \left\|\mathbf{x}_{\mathrm{rx}}\right\|=0.\end{cases}\tag{12}$$

For all possible values of path loss exponent α, the above results are in fact congruent to the analysis reported in [18].

B. Reliability for Blind Urban Intersections

For the urban intersection, we proceed by plugging the path loss model of (4) into (6). The components along roads-x and y are provided by the following propositions.

Proposition 3. The function $\mathcal{P}_{\circ}\left(\Phi_{\mathrm{x}}\right)=\exp\left(-p_{\mathrm{I}}\lambda_{\mathrm{x}}\zeta_{\mathrm{u}}\mathcal{X}\left(R_{\mathrm{x}}\right)\right)$, where $\mathcal{X}\left(R_{\mathrm{x}}\right)$ due to bounded PPP interferers on road-x evaluated for urban intersection is similar to (9), except the variable ζ_{s} is replaced by

$$\zeta_{\mathrm{u}}=\left(A_{\circ}\beta_{\mathrm{u}}^{\prime}\right)^{1/\alpha}=\left(A_{\circ}\beta/\ell_{\mathrm{pl}}^{\mathrm{u}}\left(\mathbf{x}_{\mathrm{tx}},\mathbf{x}_{\mathrm{rx}}\right)\right)^{1/\alpha}, \tag{13}$$

where the channel model $\ell_{\mathrm{pl}}^{\mathrm{u}}\left(\mathbf{x}_{\mathrm{tx}},\mathbf{x}_{\mathrm{rx}}\right)$ is characterized in (4).

Proof: Similar to Appendix A, with the exception that the contribution from the wanted signal should take into account the path loss model for the urban intersection with NLOS, WLOS or LOS; thus, ζ_{s} is replaced by ζ_{u} shown in (13). ■

Proposition 4. The function $\mathcal{P}_{\circ}\left(\Phi_{\mathrm{y}}\right)=\exp\left(-p_{\mathrm{I}}\lambda_{\mathrm{y}}\zeta_{\mathrm{u}}\mathcal{Y}\left(R_{\mathrm{y}}\right)\right)$, where $\mathcal{Y}\left(R_{\mathrm{y}}\right)$ due to bounded PPP interferers on road-y tailored for urban intersection evaluates to

$$\begin{aligned}\mathcal{Y}\left(R_{\mathrm{y}}\right)=2\Bigg(&g_{\circ}\Big(\alpha,\left(R_{\mathrm{y}}+\left\|\mathbf{x}_{\mathrm{rx}}\right\|\right)/\zeta_{\mathrm{u}}\Big)\mathbf{1}_{\left\|\mathbf{x}_{\mathrm{rx}}\right\|\leq\triangle}\\&+\Bigg(g_{\circ}\Big(\alpha,\left(\triangle+\left\|\mathbf{x}_{\mathrm{rx}}\right\|\right)/\zeta_{\mathrm{u}}\Big)+\frac{1}{\kappa}\Bigg(g_{\circ}\Big(\alpha,\kappa R_{\mathrm{y}}/\zeta_{\mathrm{u}}\Big)\\&-g_{\circ}\Big(\alpha,\kappa\triangle/\zeta_{\mathrm{u}}\Big)\Bigg)\Bigg)\mathbf{1}_{\left\|\mathbf{x}_{\mathrm{rx}}\right\|>\triangle}-g_{\circ}\Big(\alpha,\left\|\mathbf{x}_{\mathrm{rx}}\right\|/\zeta_{\mathrm{u}}\Big)\Bigg),\end{aligned} \tag{14}$$

where ζ_{u} is given in (13), $\kappa=\left(A_{\circ}/A_{\circ}^{\prime}\right)^{1/\alpha}\left\|\mathbf{x}_{\mathrm{rx}}\right\|$, $\triangle$ is the break-point distance of the urban intersection path loss, and the function $g_{\circ}\left(\alpha,\vartheta\right)$ is defined in (A.4).

Proof: See Appendix C. ■

Remark 5. It is possible to show that degradation for an urban intersection with infinite H-PPPs along roads-x and y is $\mathcal{P}_{\circ}^{\infty}\left(\Phi_{\mathrm{x}}\right)=\exp\left(-p_{\mathrm{I}}\lambda_{\mathrm{x}}\zeta_{\mathrm{u}}\mathcal{X}_{\infty}\right)$ and $\mathcal{P}_{\circ}^{\infty}\left(\Phi_{\mathrm{y}}\right)=\exp\left(-p_{\mathrm{I}}\lambda_{\mathrm{y}}\zeta_{\mathrm{u}}\mathcal{Y}_{\infty}\right)$, where $\mathcal{X}_{\infty}$ is identical to (11), and

$$\begin{aligned}\mathcal{Y}_{\infty}=2\Bigg(&\Big(\pi\csc\big(\pi/\alpha\big)/\alpha\Big)\mathbf{1}_{\left\|\mathbf{x}_{\mathrm{rx}}\right\|\leq\triangle}\\&+\Bigg(g_{\circ}\Big(\alpha,\left(\triangle+\left\|\mathbf{x}_{\mathrm{rx}}\right\|\right)/\zeta_{\mathrm{u}}\Big)+\frac{1}{\kappa}\Bigg(\pi\csc\big(\pi/\alpha\big)/\alpha\\&-g_{\circ}\Big(\alpha,\kappa\triangle/\zeta_{\mathrm{u}}\Big)\Bigg)\Bigg)\mathbf{1}_{\left\|\mathbf{x}_{\mathrm{rx}}\right\|>\triangle}-g_{\circ}\Big(\alpha,\left\|\mathbf{x}_{\mathrm{rx}}\right\|/\zeta_{\mathrm{u}}\Big)\Bigg).\end{aligned} \tag{15}$$

C. Network Analysis and Design

To ensure a tolerable worst-case level of average performance, the success probability must achieve a certain preassigned target value $\mathcal{P}_{\text{target}} \in (0,1)$, generally close to 1, such that

$$\mathcal{P}_{\text{noint}} \mathcal{P}_{\circ}\left(\Phi_{\text{x}}\right) \mathcal{P}_{\circ}\left(\Phi_{\text{y}}\right) \geq \mathcal{P}_{\text{target}} \tag{16}$$

over the intersection deployment region specified by $\mathcal{B}_{\text{x}} \cup \mathcal{B}_{\text{y}}$, and for all V2V communications pair under consideration with positions $\mathbf{x}_{\text{tx}}$ and $\mathbf{x}_{\text{rx}}$. As design parameters, we consider the transmit probability p_{I} and its relation to road segments R_{x} and R_{y}. Solving for the transmit probability in this design criteria, we find that $p_{\text{I}} \leq p_{\text{I}}^{*}\left(R_{\text{x}}, R_{\text{y}}\right)$, where the optimum probability is

$$p_{\text{I}}^{*}\left(R_{\text{x}}, R_{\text{y}}\right) = \frac{\ln(\mathcal{P}_{\text{noint}}) - \ln(\mathcal{P}_{\text{target}})}{\zeta\big(\lambda_{\text{x}} \mathcal{X}\left(R_{\text{x}}\right) + \lambda_{\text{y}} \mathcal{Y}\left(R_{\text{y}}\right)\big)}, \tag{17}$$

provided the natural condition $\mathcal{P}_{\text{target}} \leq \mathcal{P}_{\text{noint}}$ is met. Depending on the particular suburban or urban environment under design, we assign in (17) the pertinent variables for ζ and the appropriate channel model for $\ell_{\text{pl}}\left(\mathbf{x}_{\text{tx}}, \mathbf{x}_{\text{rx}}\right)$.

Evidently, it is possible to show that the minimum of $p_{\text{I}}^{*}\left(R_{\text{x}}, R_{\text{y}}\right)$ is associated with infinite H-PPPs evaluated with $\mathcal{X}_{\infty}$ and $\mathcal{Y}_{\infty}$, which we designate by $p_{\text{I}}^{\infty} \triangleq \lim_{R_{\text{x}}, R_{\text{y}} \to \infty} p_{\text{I}}^{*}\left(R_{\text{x}}, R_{\text{y}}\right)$. Under the special case where the roads are of the same dimension, i.e., $R_{\text{x}} = R_{\text{y}} = R$, the optimum transmit probability simply becomes $p_{\text{I}}^{*}\left(R\right)$, which we plot in Fig. 3 (with full simulation details provided in the next section). We observe that $p_{\text{I}}^{*}\left(R\right)$ is monotonically decreasing in R, since a larger region of possible transmitters requires a reduction in the transmit probability in order to achieve the target performance. It is interesting to note that as R becomes larger, the inverse proportionality reaches a plateau characterized by a horizontal asymptote at p_{I}^{∞}. Also, as $\mathcal{P}_{\text{target}}$ increases, the fraction of active vehicles that can transmit simultaneous to the wanted TX/RX link decreases. While keeping the same performance target, due to the communications channel quality, more vehicles can be active in the suburbs than in the city. Last, we should also be mindful that the curves represent the optimum transmit probability, which means that for a certain $R = R_{\circ}$, we could in fact choose any p_{I} below $p_{\text{I}}^{*}\left(R_{\circ}\right)$ to meet the target. Values above the curve do not meet the performance target.

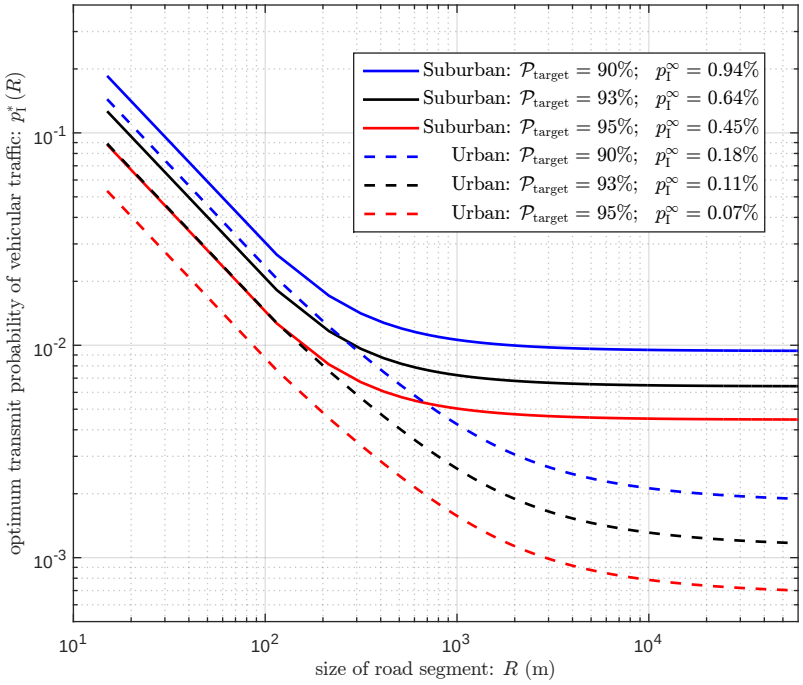

Fig. 3. Optimal transmit probability as a function of road segment $R \geq \triangle$, over different values of target reliability $\mathcal{P}_{\text{target}}$, for suburban and urban channels. These curves are based on the worst-case TX and RX positions for reliable V2V communications around the intersection, i.e., $d_{\max} = 100\,\text{m}$. The asymptotic transmit probability p_{I}^{∞} is associated to an infinite number of interfering vehicles.

V. Simulations and Discussion

A. Simulation Setup

Using the parameters shown in Table I, we evaluate the success probability under various conditions and scenarios. In particular, we set the vehicular traffic on both roads to be the same, i.e., $\lambda_{\text{x}} = \lambda_{\text{y}} = \lambda = 0.01\,\text{\#/m}$. For identical road segments $R_{\text{x}} = R_{\text{y}} = R$, we consider $R \in \{\mathcal{R}_{\text{p}}, \mathcal{R}_{\text{s}}\}$ containing a subset of practical values for real-world analysis and deployment: $\mathcal{R}_{\text{p}} \in \{200, 500\}\,\text{m}$; and another subset utilized for stress-test analysis and fundamental limits: $\mathcal{R}_{\text{s}} \in \{10, \infty\}\,\text{km}$.

Next, we assume a fixed RX on the horizontal, with $\mathbf{x}_{\text{rx}} = [-50, 0]^{\text{T}}\,\text{m}$; and a TX that could take different positions, up to a Manhattan separation of $d_{\max} = 140\,\text{m}$ away from the RX; i.e., curving around the corner and going upward on the y-road. Due to the nature of the urban channel model, we actually require, for analysis and simulations, the spatial coordinates of the

TABLE I

SIMULATION PARAMETERS

system parameters	
target success probability	$\mathcal{P}_{\rm target} = 0.9$
transmit power	$P_\circ = 20\,$dBmW
AWGN floor	$N_\circ = -99\,$dBmW
RX sensitivity	$\beta = 8\,$dB (if $B = 40\,$MHz; $r_{\rm th} \simeq 115\,$Mbps)
fixed Aloha transmit probability	$p_{\rm I} = 0.02\,$(without network design)
channel propagation	
operating frequency	$f_\circ = 5.9\,$GHz
reference distance	$d_\circ = 10\,$m
break-point distance	$\triangle = 15\,$m
path loss exponent	$\alpha = 2\,$(suburban); $1.68\,$(urban)
LOS/WLOS path loss coefficient	$A_\circ = -37.86 + 10\alpha$ dBm
NLOS path loss coefficient	$A'_\circ = -38.32 + (7 + 10\log_{10}\triangle)\alpha$ dBm
vehicular traffic and geometry	
traffic intensity	$\lambda = 0.01\,\#/\,$m
size of road segment	$R = 200\,$m (practical); $10\,$km (stress-test)
RX distance from junction point	$\|\mathbf{x}_{\rm rx}\| = 50\,$m
max. separation for reliable V2V com.	$d_{\rm target} = 100\,$m (l_1-norm distance)
max. TX/RX Manhattan separation	$d_{\max} = 140\,$m
Monte Carlo evaluation	
reliability resolution	$m_e/d_{\max} = 1\,$evaluation$\,/\,$m
H-PPP realizations	$n_{\rm PPP} = 10,000$
fading iterations	$n_{\rm f} = 5,000$
histogram bins	$n_{\rm b} = 150$

various TX positions specified by $m_{\rm e} \in \mathbb{N}_{>0}$ equidistant points, i.e.,

$$\mathbf{x}_{\rm tx}(k) = (k d_{\max}/m_{\rm e} - \|\mathbf{x}_{\rm rx}\|)\left(\mathbf{1}_{k\in\mathcal{K}_{\rm x}}\mathbf{e}_{\rm x} + \mathbf{1}_{k\in\mathcal{K}_{\rm y}}\mathbf{e}_{\rm y}\right), \tag{18}$$

for $k \in \mathcal{K}_{\rm x} \cup \mathcal{K}_{\rm y}$, and where $m_x = \lfloor m_{\rm e}\,\|\mathbf{x}_{\rm rx}\|\,/d_{\max}\rfloor$, $\mathcal{K}_{\rm x} = \{k \in \mathbb{N} \;\big|\; 1 \le k \le m_x;\ m_x > 0\}$ and $\mathcal{K}_{\rm y} = \{k \in \mathbb{N} \;\big|\; (m_x + 1) \le k \le m_{\rm e};\ m_{\rm e} > m_x\}$.

B. Sensitivity of Average Reliability to TX/RX Separation

Equipped with the above simulation setup, in this subsection, we evaluate the sensitivity of the average success probability when the TX and RX are in different locations. In particular,

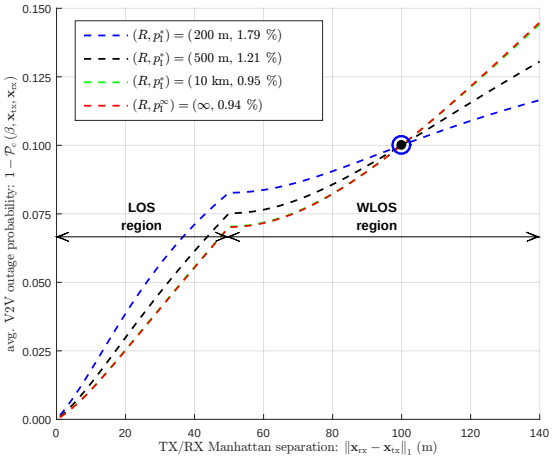

(a) sensitivity of outage probability over suburban corners

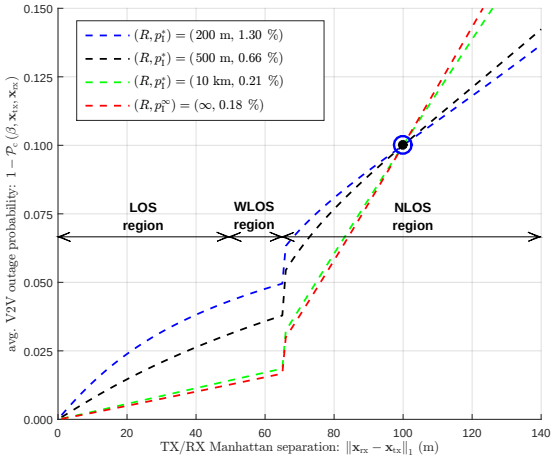

(b) sensitivity of outage probability over blind urban intersections

Fig. 4. Average reliability as a function of TX/RX separation for different channel environments and network design choices; whereby the optimum transmit probability $p_{\rm I}^*\left(R\right)$ is designed to meet a target reliability of $\mathcal{P}_{\rm target}=0.9$, at the largest V2V separation of $d_{\rm target}=100\,\text{m}$ for reliable communications.

we design the network by considering the guidelines specified by $p_{\rm I}^*\left(R\right)$, while also taking into account the maximum Manhattan separation for reliable V2V communications. That is, $d_{\rm target}=\left\|\mathbf{x}_{\rm rx}-\tilde{\mathbf{x}}_{\rm tx}\right\|_1=100\,\text{m}$, where $\|\cdot\|_1$ denotes the l_1-norm, and $\tilde{\mathbf{x}}_{\rm tx}$ is the position of the TX at the target, which in this case corresponds to $\tilde{\mathbf{x}}_{\rm tx}=50\,\mathbf{e}_{\rm y}$. As a result, we inevitably anticipate that the average reliability meets the target for different TX positions, i.e.,

$$\mathcal{P}_{\rm c}\left(\beta, \mathbf{x}_{\rm tx}, \mathbf{x}_{\rm rx}\right) \geq \mathcal{P}_{\rm c}\left(\beta, \tilde{\mathbf{x}}_{\rm tx}, \mathbf{x}_{\rm rx}\right) = \mathcal{P}_{\rm target}, \tag{19}$$

when the RX is fixed, and provided $\left\|\mathbf{x}_{\rm rx}-\mathbf{x}_{\rm tx}\right\|_1 \leq \left\|\mathbf{x}_{\rm rx}-\tilde{\mathbf{x}}_{\rm tx}\right\|_1$.

For visualization purposes, we plot in Fig. 4, the average outage probability as a function of TX/RX Manhattan separation, designed[4] for $d_{\rm target}=100\,\text{m}$, sweeping different road segments R, and over suburban and urban channel environments. We first note that when $\left\|\mathbf{x}_{\rm rx}-\mathbf{x}_{\rm tx}\right\|_1 = d_{\rm target}$, a reliability of 0.9 (shown with a blue circle mark, for a corresponding outage of 0.1) is achieved. When $\left\|\mathbf{x}_{\rm rx}-\mathbf{x}_{\rm tx}\right\|_1 < d_{\rm target}$, the outage reduces, while for $\left\|\mathbf{x}_{\rm rx}-\mathbf{x}_{\rm tx}\right\|_1 > d_{\rm target}$, the outage increases. We note that the smallest interference region (i.e., $R=200\,\text{m}$) corresponds to the largest transmit probability at target. Also, this smallest interference region leads to the

[4]For other design criteria, such as $d_{\rm target} \in \left\{20, 40, 60, 80, 120\right\}\text{m}$, which equivalently corresponds to $\tilde{\mathbf{x}}_{\rm tx} \in \left\{-30\,\mathbf{e}_{\rm x}, -10\,\mathbf{e}_{\rm x}, 10\,\mathbf{e}_{\rm y}, 30\,\mathbf{e}_{\rm y}, 70\,\mathbf{e}_{\rm y}\right\}$, sensitivity in an urban channel is available in [23].

largest outages for $\|\mathbf{x}_{\rm rx}-\mathbf{x}_{\rm tx}\|_1 < d_{\rm target}$, though never surpassing 0.1. This is due to the larger possibility of active transmitters in close proximity to the typical user, i.e., the RX. On the other hand, the smallest interference region leads to the *smallest* outages for $\|\mathbf{x}_{\rm rx}-\mathbf{x}_{\rm tx}\|_1 > d_{\rm target}$. This is because the outage is dominated by the aggregate interference, rather than the interferers close to the RX. Hence, the larger deployment region, which has more interferers, has the largest outages. Ultimately, it is important to emphasize that a small interference region allows for a high density of active transmitters $\lambda p_{\rm I}^{*}(R)$, while leading to relatively graceful degradation outside the interference region. We also notice that when we consider a very large deployment region, say $R=10\,$km, the curves nearly overlap the fundamental case for infinite region, and so this value is a feasible choice for stress-test analysis.

The outage sensitivity varies with a distinctive format as the TX moves across different regions, which is consistent with the uniqueness of the intersection path loss models. For the suburban case, there are two regions: (i) LOS: $\|\mathbf{x}_{\rm rx}-\mathbf{x}_{\rm tx}\|_1 \in \big(0, \|\mathbf{x}_{\rm rx}\|\big]$; and (ii) WLOS: $\|\mathbf{x}_{\rm rx}-\mathbf{x}_{\rm tx}\|_1 \in \big(\|\mathbf{x}_{\rm rx}\|, d_{\max}\big]$. On the other hand, for the urban case, the TX undergoes three regions: (i) LOS: $\|\mathbf{x}_{\rm rx}-\mathbf{x}_{\rm tx}\|_1 \in \big(0, \|\mathbf{x}_{\rm rx}\|\big]$; (ii) WLOS: $\|\mathbf{x}_{\rm rx}-\mathbf{x}_{\rm tx}\|_1 \in \big(\|\mathbf{x}_{\rm rx}\|, \|\mathbf{x}_{\rm rx}\|+\triangle\big]$; and (iii) NLOS: $\|\mathbf{x}_{\rm rx}-\mathbf{x}_{\rm tx}\|_1 \in \big(\|\mathbf{x}_{\rm rx}\|+\triangle, d_{\max}\big]$. As expected, the results reveal a significant deterioration of the communications reliability as the TX transitions from LOS to WLOS, and towards NLOS. Moreover, due to the non-continuous nature of the urban channel model in (4), the outage curves show an abrupt transition when $\|\mathbf{x}_{\rm rx}-\mathbf{x}_{\rm tx}\|_1 = \|\mathbf{x}_{\rm rx}\|+\triangle$, i.e. at the passing from the WLOS to the NLOS region, which in this case corresponds to a separation of $65\,$m.

Overall, our analysis of the average reliability indicates that when a system is designed for a certain maximum communication range (e.g., $d_{\rm target}=100\,$m), it is recommended to set the deployment region R as low as possible (in this case, $R=200\,$m is recommended), as this leads to the highest density of active transmitters and a graceful performance degradation outside the interference region (i.e., when $R>200\,$m). Furthermore, for a particular target performance, a better channel environment with less hindering obstacles, such as the case with suburban corners, can tolerate more active interfering nodes (i.e., a larger $p_{\rm I}^{*}$) than in built-up blind urban intersections, where the transmission quality is severely degraded over a relatively short communications distance.

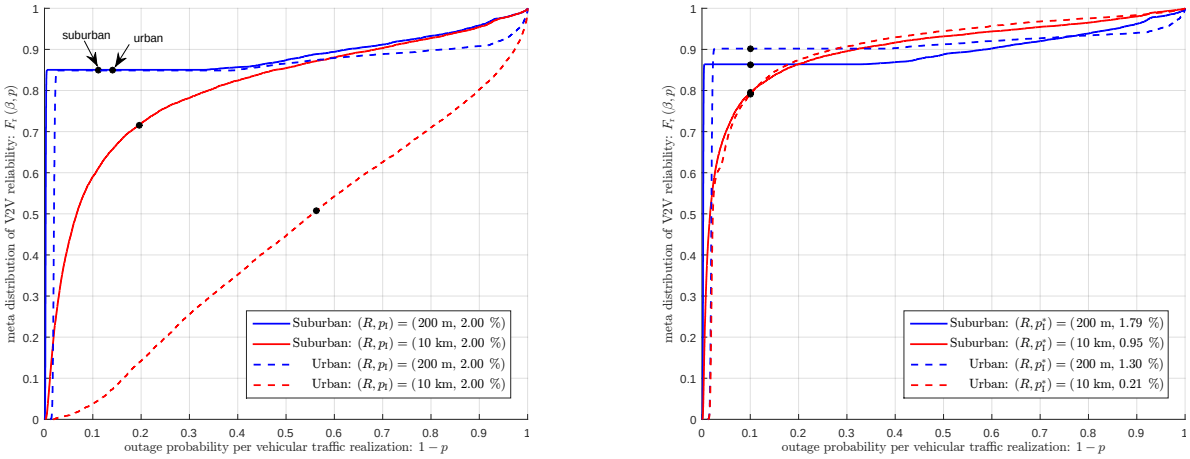

(a) meta distribution without network design: $p_{\mathrm{I}} = 0.02$

(b) meta distribution with network design: $p_{\mathrm{I}}^*(R)$

Fig. 5. Meta distribution of reliability as a function of outage probability conditioned on vehicular traffic realization under two network scenarios: (a) without design, and (b) with design. For each channel environment, the fraction of vehicular traffic is shown for $R = 200$ m (practical) and $R = 10$ km (stress-test). TX and RX are on orthogonal roads, 50 m away from the junction. The dots on the distribution curves represent the Palm expectation.

C. Sensitivity of Meta Distribution to Network Design

In the previous subsection, we analyzed the reliability averaged over point processes of the vehicular traffic and the randomness of the channel. Examining this average reliability metric is insightful, yet it is incomplete. For instance, say we consider $n_{\mathrm{PPP}} = 10,000$ traffic realizations, we are then intrigued to know: *how many of these realizations actually meet the preset requirement for target reliability* $\mathcal{P}_{\mathrm{target}}$*?* The meta distribution defined in (8) quantifies the fraction of traffic realizations that achieve a reliability constraint. In other words, the answer to the above question is: $\lfloor n_{\mathrm{PPP}} F_{\mathrm{r}}(\beta, \mathcal{P}_{\mathrm{target}}) \rfloor$.

To understand the sensitivity to network design, we consider the meta distribution for two cases: (i) without the application of network design, i.e., transmit probability is fixed at all times to $p_{\mathrm{I}} = 0.02$; and (ii) with network design guidelines applied through $p_{\mathrm{I}}^*(R)$. The setup for the simulation is similar as before, and where the TX and RX are both fixed 50 m away from the junction. Of course, the random vehicular traffic on the intersection roads vary for each of the $n_{\mathrm{PPP}} = 10,000$ realizations. Meanwhile, for each realization, we determine the related outage value, estimated via Monte Carlo techniques based on $n_{\mathrm{f}} = 5,000$ fading iterations. Once this process is completed for the $10,000$ realizations, we then assemble the outage data and build an

$n_{\mathrm{b}} = 150$ bin histogram for the probability mass function, from which a CDF plot of the meta distribution is obtained. This is shown in Fig. 5 for different design options, channels, and road segments. From analysis, we know that $\mathbb{E}^o\left(p_{\mathrm{out}}\left(\beta\right)\right) = 1 - \mathbb{E}^o\left(p_{\mathrm{c}}\left(\beta\right)\right) = 1 - \mathcal{P}_{\mathrm{c}}\left(\beta, \mathbf{x}_{\mathrm{tx}}, \mathbf{x}_{\mathrm{rx}}\right)$, shown as dots in Fig. 5.

Comparing the subfigures in Fig. 5, we observe that when network design is not applied, the average outage $1 - \mathcal{P}_{\mathrm{c}}\left(\beta, \mathbf{x}_{\mathrm{tx}}, \mathbf{x}_{\mathrm{rx}}\right)$ varies from 0.56 (urban, $R = 10\,\mathrm{km}$) to 0.11 (suburban, $R = 200\,\mathrm{m}$). The corresponding meta distribution $F_{\mathrm{r}}\left(\beta, \mathcal{P}_{\mathrm{c}}\left(\beta, \mathbf{x}_{\mathrm{tx}}, \mathbf{x}_{\mathrm{rx}}\right)\right)$ varies between 0.51 to 0.85, indicating that for the urban intersection with $R = 10\,\mathrm{km}$ about half the PPP realizations achieve the target reliability $\mathcal{P}_{\mathrm{c}}\left(\beta, \mathbf{x}_{\mathrm{tx}}, \mathbf{x}_{\mathrm{rx}}\right)$, while this number increases to nearly 90% for the suburban intersection at $R = 200\,\mathrm{m}$. In other words, for small value of R, the meta-distribution exhibits a bimodal behavior, characterized by a large number of "good" PPPs and a small number of "bad" PPPs, meaning the traffic realizations lead to either very reliable or extremely unreliable communication conditions. When network design is applied (see Fig. 5b), $\mathbb{E}^o\left(p_{\mathrm{out}}\left(\beta\right)\right) = 1 - \mathcal{P}_{\mathrm{c}}\left(\beta, \mathbf{x}_{\mathrm{tx}}, \mathbf{x}_{\mathrm{rx}}\right) = 1 - \mathcal{P}_{\mathrm{target}} = 0.1$, while $F_{\mathrm{r}}\left(\beta, \mathcal{P}_{\mathrm{target}}\right) = F_{\mathrm{r}}\left(\beta, 0.9\right)$ ranges from 0.8 to 0.9, meaning that a greater fraction of traffic realizations achieve the target reliability when compared to the case of no design. Note that when $R = 200\,\mathrm{m}$ in Fig. 5b, the meta distribution for the urban channel is slightly higher than for the suburban channel since, due to design, the suburban case allows a higher value of transmit probability, i.e., more simultaneously active vehicles are tolerated. Moreover, for $R = 200\,\mathrm{m}$, the meta distribution is again bimodal, while for $R = 10\,\mathrm{km}$ it is not. Overall, these results indicate that the average performance alone is not an adequate metric to assess communication reliability, but with different reasons for large and small transmission ranges.

D. Sensitivity of Fine-grained Reliability to TX/RX Separation

In the previous subsection, we looked at the meta distribution of reliability. Here, we also aim to obtain the meta distribution as a function of $\mathbf{x}_{\mathrm{tx}}$ and $\mathbf{x}_{\mathrm{rx}}$, obtained from the fine-grained reliability plots, i.e., outage probability per traffic realization as a function of TX/RX Manhattan separation. We consider the same setup explained in the previous section (now designed for $d_{\mathrm{target}} = 100\,\mathrm{m}$ and $\mathcal{P}_{\mathrm{target}} = 0.9$) to obtain an outage value for each realization. However, here, the RX will remain fixed at $\mathbf{x}_{\mathrm{rx}} = -50\,\mathbf{e}_{\mathrm{x}}$, and the TX will have different positions with a reliability resolution of $m_e / d_{\max} = 1\,\text{evaluation}\,/\,\mathrm{m}$. For every TX/RX position pair, we obtain $10,000$ outage values. Therefore, we have to do this process over many times to get a fine-

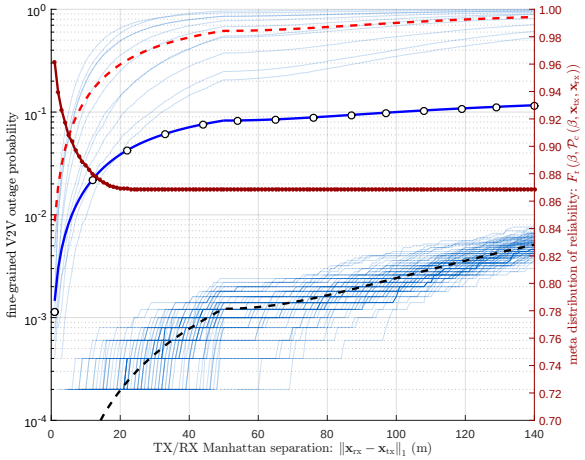

(a) fine-grained reliability, suburban corners: $R = 200\,\mathrm{m}$

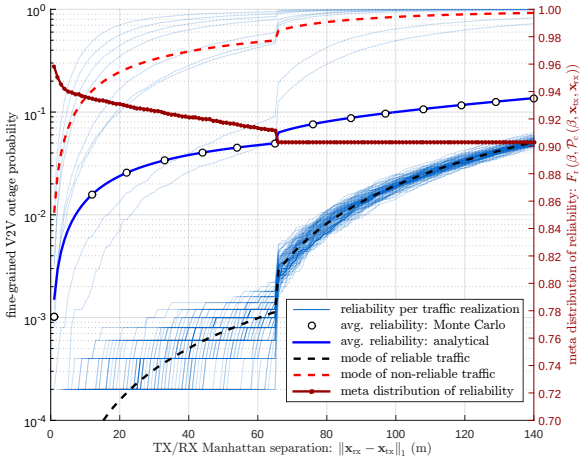

(b) fine-grained reliability, blind urban intersections: $R = 200\,\mathrm{m}$

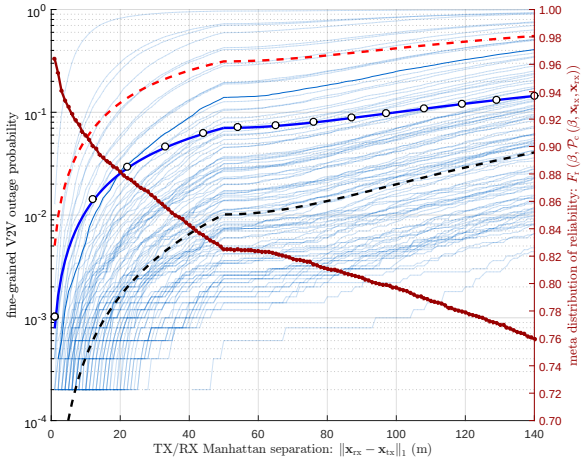

(c) fine-grained reliability, suburban corners: $R = 10\,\mathrm{km}$

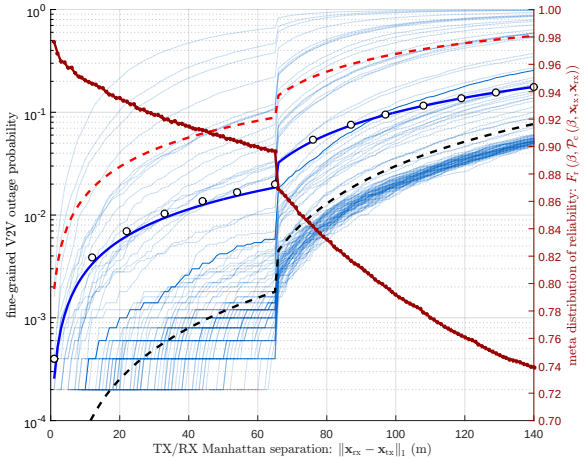

(d) fine-grained reliability, blind urban intersections: $R = 10\,\mathrm{km}$

Fig. 6. Fine-grained reliability under network design as a function of TX/RX separation for different channel environments and road segments. The analysis is based on $n_{\mathrm{ppp}} = 10,000$, however for illustration purposes, we only show the first 100 fine-grained outage curves evaluated using Monte Carlo simulation, where each fine-line is associated with a certain vehicular traffic realization. The average reliability is then estimated and compared to the analytically derived expressions. The mode for reliable and non-reliable traffic identified at target reliability $(d_{\mathrm{target}}, 1 - \mathcal{P}_{\mathrm{target}}) = (100\,\mathrm{m}, 0.1)$ are plotted. The meta distribution of reliability is also shown for different V2V separations.

grained reliability, i.e., $m_e \times n_{\mathrm{ppp}} = 140 \times 10,000 = 1.4\,\mathrm{Million}$ outage values that must be estimated, and where each of these values is averaged over $n_{\mathrm{f}} = 5,000$ fading iterations.

Similar to Fig. 4, in Fig. 6, we plot the average outage $1 - \mathcal{P}_{\mathrm{c}}(\beta, \mathbf{x}_{\mathrm{tx}}, \mathbf{x}_{\mathrm{rx}})$ (with an axis on the left), and the meta distribution $F_{\mathrm{r}}(\beta, \mathcal{P}_{\mathrm{c}}(\beta, \mathbf{x}_{\mathrm{tx}}, \mathbf{x}_{\mathrm{rx}}))$ (with an axis on the right) both as

a function of $\|\mathbf{x}_{\mathrm{rx}} - \mathbf{x}_{\mathrm{tx}}\|_1$. With increasing $\|\mathbf{x}_{\mathrm{rx}} - \mathbf{x}_{\mathrm{tx}}\|_1$, $1 - \mathcal{P}_{\mathrm{c}}(\beta, \mathbf{x}_{\mathrm{tx}}, \mathbf{x}_{\mathrm{rx}})$ increases, while $F_{\mathrm{r}}(\beta, \mathcal{P}_{\mathrm{c}}(\beta, \mathbf{x}_{\mathrm{tx}}, \mathbf{x}_{\mathrm{rx}}))$ decreases. Both of these phenomena are a natural V2V communications response, as the TX vehicle transitioning from the LOS region to the WLOS region, and finally onto the NLOS region around the blind-intersection. In other words, the overall trend for average reliability and fine-grained reliability indicate a deterioration of the communications quality. Also, in Figs. 6a–6b, after a certain TX/RX separation, the meta distribution reaches a steady-state, which is a clear indication of the bimodal behavior for small values of road segments.

Although averaged over $10,000$ realizations, for visualization purposes, we only show the fine-grained reliability for 100 randomly drawn traffic realizations. The bimodal behavior for $R = 200\,\mathrm{m}$ is again clearly visible: we have either very reliable traffic realizations or (by design, fewer) non-reliable realizations, but nowhere in close proximity to the average measure. For the more realistic range of $R = 200\,\mathrm{m}$, outage is mainly determined by the presence or absence of interferers, while for $R = 10\,\mathrm{km}$, outage is mainly determined by the distance to the closest interferers. Grouping the 10,000 realizations based on whether or not they meet the target, we can compute conditional outage probabilities, shown as dashed lines. For $R = 10\,\mathrm{km}$, these lines are a measure of the spread of the meta distribution around the mean, while for $R = 200\,\mathrm{m}$, the dashed lines are an indication of the separation between the two modes of the meta distribution.

Overall, we find that the generally accepted notion that reliability for a particular traffic realization will be in relative proximity to the average is utterly misleading. In fact, in this case, averages are essentially an oversimplified distortion of reality. They provide ballpark values, but these values may not necessarily exist for a particular vehicular traffic scenario as shown here.

VI. Conclusion

V2V communication is critical for future intelligent transportation systems. A key performance metric is the probability of successful packet delivery in the presence of interference. In this paper, we analytically characterized the success probability for suburban and urban intersections based on specialized path loss models. It turns out that these path loss models are amenable for mathematical analysis and lead to exact closed-form expressions for different path loss exponents and finite interference regions. The derived expressions can aid in the communication system design task, complementing time-consuming simulations and experiments. In particular, we found that from a system perspective, it is beneficial to limit interference to a small spatial region, while allowing more simultaneous transmitters. We also explained the notion of network design

in order to ascertain a target reliability. This was coupled with the meta distribution, where it was shown that a small road segment can lead to a higher fraction of traffic realizations that achieve the target reliability, as compared to infinitely long roads. Finally, fine-grained reliability per traffic realization reveals a bimodal distribution outcome for practical real-world deployment over short road segments, thus indicating that traditional metrics based on averages are important, but not sufficient, for ultra-reliable applications such as V2V communications.

APPENDIX A
PROOF OF PROPOSITION 1: $\mathcal{P}_{\circ}\left(\Phi_{\mathrm{x}}\right)$ FOR SUBURBAN

We consider random interferers on road-x characterized by $\Phi_{\mathrm{x}} \sim \mathrm{PPP}\left(p_{\mathrm{I}}\lambda_{\mathrm{x}}, \mathcal{B}_{\mathrm{x}}\right)$. We substitute the channel model of (3) into (7), and since $\mathbf{x}_{\mathrm{rx}} = x_{\mathrm{rx}}\mathbf{e}_{\mathrm{x}}$ and $\mathbf{x} = x\mathbf{e}_{\mathrm{x}}$, the multidimensional integration reduces to

$$\mathcal{P}_{\circ}\left(\Phi_{\mathrm{x}}\right) = \exp\Bigg(-\int_{\mathcal{B}_{\mathrm{x}}} \frac{p_{\mathrm{I}}\lambda_{\mathrm{x}}\,\mathrm{d}x}{\left(1+\left(\left|x_{\mathrm{rx}}-x\right|/\zeta_{\mathrm{s}}\right)^{\alpha}\right)}\Bigg), \tag{A.1}$$

such that $\zeta_{\mathrm{s}} = \left(A_{\circ}\beta_{\mathrm{s}}'\right)^{1/\alpha} = \beta^{1/\alpha}\left\|\mathbf{x}_{\mathrm{rx}}-\mathbf{x}_{\mathrm{tx}}\right\|$. At present, to solve (A.1), two possible cases arise.

Case I – RX is Inside Bounded Set $\mathcal{B}_{\mathrm{x}}$: $\|\mathbf{x}_{\mathrm{rx}}\| \leq R_{\mathrm{x}}$: Due to $|x_{\mathrm{rx}}-x|$, the above integral must be split in two parts, namely

$$\mathcal{P}_{\circ}\left(\Phi_{\mathrm{x}}\right) = \exp\Bigg(-p_{\mathrm{I}}\lambda_{\mathrm{x}}\Bigg\{\int_{-R_{\mathrm{x}}}^{x_{\mathrm{rx}}} \frac{\mathrm{d}x}{\left(1+\left(\left(x_{\mathrm{rx}}-x\right)/\zeta_{\mathrm{s}}\right)^{\alpha}\right)} + \int_{x_{\mathrm{rx}}}^{R_{\mathrm{x}}} \frac{\mathrm{d}x}{\left(1+\left(\left(x-x_{\mathrm{rx}}\right)/\zeta_{\mathrm{s}}\right)^{\alpha}\right)}\Bigg\}\Bigg). \tag{A.2}$$

If we let $u = \left(x_{\mathrm{rx}}-x\right)/\zeta_{\mathrm{s}}$ for the first part, and $v = -u$ for the second, (A.2) becomes

$$\mathcal{P}_{\circ}\left(\Phi_{\mathrm{x}}\right) = \exp\Bigg(-p_{\mathrm{I}}\lambda_{\mathrm{x}}\zeta_{\mathrm{s}}\Bigg\{g_{\circ}\Big(\alpha, \frac{\left(R_{\mathrm{x}}+x_{\mathrm{rx}}\right)}{\zeta_{\mathrm{s}}}\Big)+g_{\circ}\Big(\alpha, \frac{\left(R_{\mathrm{x}}-x_{\mathrm{rx}}\right)}{\zeta_{\mathrm{s}}}\Big)\Bigg\}\Bigg), \tag{A.3}$$

where the recurring function $g_{\circ}\left(\alpha,\vartheta\right)$ is defined below. Meanwhile, we should underscore that due to the symmetry in (A.3), it is possible to replace x_{rx} by $\|\mathbf{x}_{\mathrm{rx}}\|$, while still remaining compatible when $x_{\mathrm{rx}} < 0$.

Definition 6. Let the function $g_{\circ}\left(\alpha,\vartheta\right)\!:\mathbb{R}^{+}\!\times\mathbb{R}_{0}^{+}\mapsto\mathbb{R}_{0}^{+}$ be dependent on Gauss's hypergeometric function ${}_2F_1\left(a,b;c;x\right)$ as follows

$$g_{\circ}(\alpha,\vartheta)\triangleq\int_{0}^{\vartheta}\frac{\mathrm{d}u}{(1+u^{\alpha})}=\vartheta\,{}_2F_1\Big(1,\frac{1}{\alpha};\big(1+\frac{1}{\alpha}\big);-\vartheta^{\alpha}\Big)\,. \tag{A.4}$$

For some values of $\alpha>1$, the function in (A.4) reverts to a simple form; for instance: $g_{\circ}\left(\alpha=2,\vartheta\right)=\arctan\left(\vartheta\right)$.

Case II – RX is Outside Bounded Set $\mathcal{B}_{\mathrm{x}}$: $\|\mathbf{x}_{\mathrm{rx}}\|>R_{\mathrm{x}}$: The RX must be outside the region of H-PPP interferers on road-x; therefore, we may consider $x_{\mathrm{rx}}<-R_{\mathrm{x}}$ or $x_{\mathrm{rx}}>R_{\mathrm{x}}$. Due to symmetry, the final result will be identical. As it is more evolved, here we opt to demonstrate the derivation with a RX positioned on the negative axis. Thus, we replace $|x_{\mathrm{rx}}-x|$ by $(x-x_{\mathrm{rx}})$ in (A.1), while taking the integration over $|x|\leq R_{\mathrm{x}}$; also, realizing that $-x_{\mathrm{rx}}=\|\mathbf{x}_{\mathrm{rx}}\|$, we get

$$\mathcal{P}_{\circ}\left(\Phi_{\mathrm{x}}\right)=\exp\Bigg(-\int_{-R_{\mathrm{x}}}^{R_{\mathrm{x}}}\frac{p_{\mathrm{I}}\lambda_{\mathrm{x}}\,\mathrm{d}x}{\big(1+\big(\big(x+\|\mathbf{x}_{\mathrm{rx}}\|\big)/\zeta_{\mathrm{s}}\big)^{\alpha}\big)}\Bigg). \tag{A.5}$$

If we let $u=\left(x+\|\mathbf{x}_{\mathrm{rx}}\|\right)/\zeta_{\mathrm{s}}$, the expression in (A.5) will then equal to (A.6), where $g_{\circ}\left(\alpha,\vartheta\right)$ is defined in (A.4).

$$\mathcal{P}_{\circ}\left(\Phi_{\mathrm{x}}\right)=\exp\Bigg(-p_{\mathrm{I}}\lambda_{\mathrm{x}}\zeta_{\mathrm{s}}\int_{(\|\mathbf{x}_{\mathrm{rx}}\|-R_{\mathrm{x}})/\zeta_{\mathrm{s}}}^{(\|\mathbf{x}_{\mathrm{rx}}\|+R_{\mathrm{x}})/\zeta_{\mathrm{s}}}\frac{\mathrm{d}u}{\big(1+u^{\alpha}\big)}\Bigg)= \tag{A.6}$$

$$\exp\Bigg(-p_{\mathrm{I}}\lambda_{\mathrm{x}}\zeta_{\mathrm{s}}\Big\{g_{\circ}\Big(\alpha,\frac{(\|\mathbf{x}_{\mathrm{rx}}\|+R_{\mathrm{x}})}{\zeta_{\mathrm{s}}}\Big)-g_{\circ}\Big(\alpha,\frac{(\|\mathbf{x}_{\mathrm{rx}}\|-R_{\mathrm{x}})}{\zeta_{\mathrm{s}}}\Big)\Big\}\Bigg)$$

APPENDIX B
PROOF OF PROPOSITION 2: $\mathcal{P}_{\circ}\left(\Phi_{\mathrm{y}}\right)$ FOR SUBURBAN

We analyze random interfering vehicles on road-y modeled by $\Phi_{\mathrm{y}}\sim\mathrm{PPP}\left(p_{\mathrm{I}}\lambda_{\mathrm{y}},\mathcal{B}_{\mathrm{y}}\right)$. The RX is positioned at $\mathbf{x}_{\mathrm{rx}}=x_{\mathrm{rx}}\mathbf{e}_{\mathrm{x}}$ and the interferers are located at $\mathbf{x}=y\mathbf{e}_{\mathrm{y}}$. After substituting these spatial parameters and the channel model of (3) into (7), we find that

$$\mathcal{P}_{\circ}\left(\Phi_{\mathrm{y}}\right)=\exp\Bigg(-\int_{\mathcal{B}_{\mathrm{y}}}\frac{p_{\mathrm{I}}\lambda_{\mathrm{y}}\,\mathrm{d}y}{\big(1+\big(\big(y^{2}+\|\mathbf{x}_{\mathrm{rx}}\|^{2}\big)/\zeta_{\mathrm{s}}^{2}\big)^{\alpha/2}\big)}\Bigg). \tag{B.1}$$

The above could be simplified by assigning $u=\big(y^{2}+\|\mathbf{x}_{\mathrm{rx}}\|^{2}\big)/\zeta_{\mathrm{s}}^{2}$, and thus $\mathrm{d}y=\zeta_{\mathrm{s}}^{2}\mathrm{d}u/2y$, where $y=\pm\,\zeta_{\mathrm{s}}\sqrt{u-\|\mathbf{x}_{\mathrm{rx}}\|^{2}/\zeta_{\mathrm{s}}^{2}}$. Following some manipulations, we get

$$\mathcal{P}_{\circ}\left(\Phi_{\mathrm{y}}\right)=\exp\Bigg(-p_{\mathrm{I}}\lambda_{\mathrm{y}}\zeta_{\mathrm{s}}\int_{\delta}^{R_{\mathrm{y}}^{2}/\zeta_{\mathrm{s}}^{2}+\delta}\frac{\mathrm{d}u}{\sqrt{u-\delta}\big(1+u^{\alpha/2}\big)}\Bigg), \tag{B.2}$$

such that $\delta = \|\mathbf{x}_{\rm rx}\|^2/\zeta_{\rm s}^2$. The format of the integration within (B.2) can be defined as follows.

Definition 7. Let the function $h_\circ(\alpha,\delta,\vartheta):\mathbb{R}^+\times\mathbb{R}_0^+\times\mathbb{R}_0^+\mapsto\mathbb{R}_0^+$ be defined as follows

$$h_\circ(\alpha,\delta,\vartheta)\triangleq\int_{\delta}^{\vartheta+\delta}\frac{\mathrm{d}u}{\sqrt{u-\delta}\,(1+u^{\alpha/2})}\,. \tag{B.3}$$

For values of $\alpha>1$, this integral can be solved efficiently using standard numerical methods. However, in some cases, a tractable expression for (B.3) is available, for instance

$$h_\circ(\alpha,0,\vartheta)=2\sqrt{\vartheta}\,{}_2F_1\left(1,\frac{1}{\alpha};\big(1+\frac{1}{\alpha}\big);-\vartheta^{\alpha/2}\right) \tag{B.4}$$

$$h_\circ(\alpha=2,\delta,\vartheta)=2\arctan\big(\sqrt{\vartheta/(1+\delta)}\,\big)/\sqrt{1+\delta}\,. \tag{B.5}$$

APPENDIX C
PROOF OF PROPOSITION 4: $\mathcal{P}_\circ(\Phi_{\rm y})$ FOR URBAN

We consider random interferers on road-y modeled by $\Phi_{\rm y}\sim\text{PPP}\,(p_{\rm I}\lambda_{\rm y},\mathcal{B}_{\rm y})$, where the RX and interferes are accordingly located at $\mathbf{x}_{\rm rx}=x_{\rm rx}\mathbf{e}_{\rm x}$ and $\mathbf{x}=y\mathbf{e}_{\rm y}$. Taking into account these parameters and substituting the propagation model for urban intersection of (4) into (7), we obtain

$$\mathcal{P}_\circ(\Phi_{\rm y})=\exp\bigg(-\int_{\mathcal{B}_{\rm y}}\frac{p_{\rm I}\lambda_{\rm y}\,\mathrm{d}y}{\big(1+1/\beta'_{\rm u}\ell^{\rm u}_{\rm pl}(\mathbf{x},\mathbf{x}_{\rm rx})\big)}\bigg). \tag{C.1}$$

To solve (C.1), two possible cases arise.

Case I – RX is Near the Intersection Point: $\|\mathbf{x}_{\rm rx}\|\le\triangle$*:* When the RX is closer to the intersection, the WLOS Manhattan model within (4) is the only relevant channel; thus we get

$$\mathcal{P}_\circ(\Phi_{\rm y})=\exp\bigg(-\int_{\mathcal{B}_{\rm y}}\frac{p_{\rm I}\lambda_{\rm y}\,\mathrm{d}y}{\big(1+\big(\big(|y|+\|\mathbf{x}_{\rm rx}\|\big)/\zeta_{\rm u}\big)^{\alpha}\big)}\bigg), \tag{C.2}$$

where $\zeta_{\rm u}=(A_\circ\beta'_{\rm u})^{1/\alpha}$. If we perform a change of variable to (C.2) with $u=\big(|y|+\|\mathbf{x}_{\rm rx}\|\big)/\zeta_{\rm u}$, we obtain

$$\mathcal{P}_\circ(\Phi_{\rm y})= \tag{C.3}$$
$$\exp\bigg(-2p_{\rm I}\lambda_{\rm y}\zeta_{\rm u}\Big\{g_\circ\Big(\alpha,\frac{\big(R_{\rm y}+\|\mathbf{x}_{\rm rx}\|\big)}{\zeta_{\rm u}}\Big)-g_\circ\Big(\alpha,\frac{\|\mathbf{x}_{\rm rx}\|}{\zeta_{\rm u}}\Big)\Big\}\bigg),$$

where $g_\circ(\alpha,\vartheta)$ is defined in (A.4).

Case II – RX is Away from the Intersection Point: $\|\mathbf{x}_{\rm rx}\| > \triangle$*:* In this case, the WLOS Manhattan model within (4) is relevant for $\|\mathbf{x}\| \leq \triangle$, and the NLOS VirtualSource11p model over $\triangle < \|\mathbf{x}\| \leq R_{\rm y}$. Applying these models into (C.1), we get

$$\mathcal{P}_{\circ}\left(\Phi_{\rm y}\right) = \exp\Bigg(-2p_{\rm I}\lambda_{\rm y}\Bigg\{\int_{0}^{\triangle}\frac{{\rm d}y}{\left(1+\left(\left(y+\|\mathbf{x}_{\rm rx}\|\right)/\zeta_{\rm u}\right)^{\alpha}\right)} + \int_{\triangle}^{R_{\rm y}}\frac{{\rm d}y}{\left(1+\left(y\,\|\mathbf{x}_{\rm rx}\|/\zeta'_{\rm u}\right)^{\alpha}\right)}\Bigg\}\Bigg), \tag{C.4}$$

where $\zeta_{\rm u} = \left(A_{\circ}\beta'_{\rm u}\right)^{1/\alpha}$ and $\zeta'_{\rm u} = \left(A'_{\circ}\beta'_{\rm u}\right)^{1/\alpha} = \zeta_{\rm u}\left(A'_{\circ}/A_{\circ}\right)^{1/\alpha}$. If we let $u = \left(y+\|\mathbf{x}_{\rm rx}\|\right)/\zeta_{\rm u}$ for the first integration in (C.4), and $v = y\,\|\mathbf{x}_{\rm rx}\|/\zeta'_{\rm u}$ for the second, we get

$$\mathcal{P}_{\circ}\left(\Phi_{\rm y}\right) = \exp\Bigg(-2p_{\rm I}\lambda_{\rm y}\zeta_{\rm u}\Bigg\{g_{\circ}\Big(\alpha, \frac{\left(\triangle+\|\mathbf{x}_{\rm rx}\|\right)}{\zeta_{\rm u}}\Big) - g_{\circ}\Big(\alpha, \frac{\|\mathbf{x}_{\rm rx}\|}{\zeta_{\rm u}}\Big) + \frac{1}{\kappa}\Bigg(g_{\circ}\Big(\alpha, \frac{\kappa R_{\rm y}}{\zeta_{\rm u}}\Big) - g_{\circ}\Big(\alpha, \frac{\kappa\triangle}{\zeta_{\rm u}}\Big)\Bigg)\Bigg\}\Bigg), \tag{C.5}$$

where $\kappa = \left(A_{\circ}/A'_{\circ}\right)^{1/\alpha}\|\mathbf{x}_{\rm rx}\|$ and $g_{\circ}\left(\alpha,\vartheta\right)$ is defined in (A.4).

ACKNOWLEDGMENTS

The authors are also grateful to Prof. Martin Haenggi (University of Notre Dame, IN, USA) for discussions regarding the meta distribution.

REFERENCES

[1] "Global Status Report on Road Safety," World Health Organization, specialised agency of the United Nations, Oct. 2015.

[2] "Critical reasons for crashes investigated in the National Motor Vehicle Crash Causation Survey," U.S. Dept. of Transportation, HS-812115, Feb. 2015.

[3] "Federal Automated Vehicles Policy: Accelerating the Next Revolution in Roadway Safety," U.S. Dept. of Transportation, Sep. 2016.

[4] M. Abdulla, "Self-driving vehicles: The path forward with LIDAR and V2x technologies," in *IEEE VTS/ComSoc/SPS Invited Seminar*, McGill University, Montréal, Québec, Canada, Jan. 5, 2017.

[5] "Study on the Deployment of C-ITS in Europe: Final Report," EU, European Commission, Feb. 2016.

[6] "Traffic Safety Facts 2015," U.S. Dept. of Transportation, HS-812384, Jan. 2017.

[7] "Part 11: Wireless LAN Medium Access Control (MAC) and Physical Layer (PHY) Specifications Amendment 6: Wireless Access in Vehicular Environments," IEEE 802.11p standard, Jul. 2010.

[8] "LTE, Rel.14.: Parallel feasibility study on LTE-based V2X Services," RP-151109, Malmö, Sweden, Jun. 15-18, 2015.

[9] "LTE, Rel.14, Support for V2V services based on LTE sidelink," RP-152293, Sitges, Spain, Dec. 7-10, 2015.

[10] "The Case for Cellular V2x for Safety and Cooperative Driving," 5G Automotive Association, Nov. 2016.

[11] "5G for Europe: An Action Plan," EU, European Commission, Sep. 2016.

[12] J. Choi, V. Va, N. Gonzalez-Prelcic, R. Daniels, C. R. Bhat, and R. W. Heath, "Millimeter-wave vehicular communication to support massive automotive sensing," *IEEE Communications Magazine*, vol. 54, no. 12, pp. 160–167, Dec. 2016.

[13] L. Kong, M. K. Khan, F. Wu, G. Chen, and P. Zeng, "Millimeter-wave wireless communications for IoT-cloud supported autonomous vehicles: overview, design, and challenges," *IEEE Communications Magazine*, vol. 55, no. 1, pp. 62–68, Jan. 2017.

[14] "Evolving LTE to fit the 5G future," Ericsson Technology Review, Stockholm, Sweden, Jan. 2017.

[15] B. Błaszczyszyn, P. Mühlethaler, and Y. Toor, "Performance of MAC protocols in linear VANETs under different attenuation and fading conditions," in *Proc. IEEE Conference on Intelligent Transportation Systems*, Oct. 2009, pp. 1–6.

[16] B. Błaszczyszyn, P. Mühlethaler, and N. Achir, "Vehicular ad-hoc networks using slotted Aloha: point-to-point, emergency and broadcast communications," in *Proc. IFIP Wireless Days*, Nov. 2012, pp. 1–6.

[17] Y. Jeong, J. W. Chong, H. Shin, and M. Z. Win, "Intervehicle communication: Cox-Fox modeling," *IEEE Journal on Selected Areas in Communications*, vol. 31, no. 9, pp. 418–433, Sep. 2013.

[18] E. Steinmetz, M. Wildemeersch, T. Q. Quek, and H. Wymeersch, "A stochastic geometry model for vehicular communication near intersections," in *Proc. of IEEE Globecom Workshops*, San Diego, CA, USA, Dec. 6-10, 2015, pp. 1–6.

[19] M. J. Farooq, H. ElSawy, and M. S. Alouini, "A stochastic geometry model for multi-hop highway vehicular communication," *IEEE Trans. on Wireless Communications*, vol. 15, no. 3, pp. 2276–2291, Mar. 2016.

[20] Z. Tong, H. Lu, M. Haenggi, and C. Poellabauer, "A stochastic geometry approach to the modeling of DSRC for vehicular safety communication," *IEEE Trans. on Intelligent Transportation Systems*, vol. 17, no. 5, pp. 1448–1458, May 2016.

[21] T. Kimura, H. Saito, H. Honda, and R. Kawahara, "Modeling urban ITS Communication via stochastic geometry approach," in *Proc. of the 84th IEEE Vehicular Technology Conference*, Sep. 2016, pp. 1–5.

[22] E. Steinmetz, M. Wildemeersch, T. Q. Quek, and H. Wymeersch, "Packet reception probabilities in vehicular communications close to intersections," *submitted for publication*, 2016.

[23] M. Abdulla, E. Steinmetz, and H. Wymeersch, "Vehicle-to-vehicle communications with urban intersection path loss models," in *Proc. of IEEE Globecom*, Washington DC, USA, Dec. 4-8, 2016, pp. 1–6.

[24] C. F. Mecklenbrauker, A. F. Molisch, J. Karedal, F. Tufvesson, A. Paier, L. Bernado, T. Zemen, O. Klemp, and N. Czink, "Vehicular channel characterization and its implications for wireless system design and performance," *Proc. of the IEEE*, vol. 99, no. 7, pp. 1189–1212, Jul. 2011.

[25] J. Karedal, N. Czink, A. Paier, F. Tufvesson, and A. F. Molisch, "Path loss modeling for vehicle-to-vehicle communications," *IEEE Trans. on Vehicular Technology*, vol. 60, no. 1, pp. 323–328, Jan. 2011.

[26] M. Haenggi, "The meta distribution of the SIR in poisson bipolar and cellular networks," *IEEE Trans. on Wireless Communications*, vol. 15, no. 5, pp. 2577–2589, Apr. 2016.

[27] J. Karedal, F. Tufvesson, T. Abbas, O. Klemp, A. Paier, L. Bernado, and A. F. Molisch, "Radio channel measurements at street intersections for vehicle-to-vehicle safety applications," in *Proc. of the 71st IEEE Vehicular Technology Conference*, May 2010, pp. 1–5.

[28] M. Schack, J. Nuckelt, R. Geise, L. Thiele, and T. Kürner, "Comparison of path loss measurements and predictions at urban crossroads for C2C communications," in *Proc. of the 5th European Conference on Antennas and Propagation (EuCAP)*, Apr. 2011, pp. 2896–2900.

[29] T. Mangel, O. Klemp, and H. Hartenstein, "5.9 GHz inter-vehicle communication at intersections: a validated non-line-of-sight pathloss and fading model," *EURASIP Journal on Wireless Communications and Networking*, pp. 1–11, Nov. 2011.

[30] T. Abbas, A. Thiel, T. Zemen, C. F. Mecklenbrauker, and F. Tufvesson, "Validation of a non-line-of-sight path-loss model

for V2V communications at street intersections," in *Proc. of the 13th International Conference on ITS Telecommunications (ITST'13)*, Tampere, Finland, Nov. 5-7, 2013, pp. 198–203.

[31] N. Ross and D. Schuhmacher, "Wireless network signals with moderately correlated shadowing still appear poisson," *IEEE Trans. on Information Theory*, vol. 63, no. 2, pp. 1177–1198, Feb. 2017.

[32] B. Błaszczyszyn and H. Keeler, "Equivalence and comparison of heterogeneous cellular networks," in *Proc. of the 24th IEEE International Symposium on Personal, Indoor and Mobile Radio Communications (PIMRC Workshops)*, Sep. 2013, pp. 153–157.

[33] "5G Automotive Vision," 5G Public Private Partnership, Oct. 2015.

[34] G. Durisi, T. Koch, and P. Popovski, "Toward massive, ultrareliable, and low-latency wireless communication with short packets," *Proc. of the IEEE*, vol. 104, no. 9, pp. 1711–1726, Sep. 2016.

[35] Y. Polyanskiy, H. V. Poor, and S. Verdu, "Channel coding rate in the finite blocklength regime," *IEEE Trans. on Information Theory*, vol. 56, no. 5, pp. 2307–2359, May 2010.

[36] J. Gil-Pelaez, "Note on the inversion theorem," *Biometrika*, vol. 38, no. 3-4, pp. 481–482, 1951.

[37] M. Salehi, A. Mohammadi, and M. Haenggi, "Analysis of D2D underlaid cellular networks: SIR meta distribution and mean local delay," *accepted, IEEE Trans. on Communications*, 2017.

[38] Y. Wang, M. Haenggi, and Z. Tan, "The meta distribution of the SIR for cellular networks with power control," *submitted for publication*, 2017.